Depth, distribution, and density of CO_2 deposition on Mars

Oded Aharonson,[1] Maria T. Zuber,[2,3] David E. Smith,[3] Gregory A. Neumann,[2,3] William C. Feldman,[4] and Thomas H. Prettyman[4]

Received 6 December 2003; revised 5 February 2004; accepted 29 March 2004; published 20 May 2004.

[1] Observations by the Mars Orbiter Laser Altimeter have been used to detect subtle changes of the polar surface height during the course of seasonal cycles that correlate with the expected pattern of CO_2 deposition and sublimation. Using altimetric crossover residuals from the Mars Orbiter Laser Altimeter, we show that while zonally averaged data capture the global behavior of CO_2 exchange, there is a dependence of the pattern on longitude. At the highest latitudes the surface height change is as high as 1.5–2 m peak to peak, and it decreases equatorward. Decomposition of the signal into harmonics in time allows inspection of the spatial pattern and shows that the annual component is strongly correlated with the residual south polar cap deposits and, to a lesser extent, with the north polar cap. In the north, the second harmonic (semiannual) component correlates with the location of the ice deposits. The phases of the annual cycles are in agreement with observations by the Thermal Emission Spectrometer of the timing of the annual disappearance of CO_2 frost from the surface at the high latitudes. At lower latitudes, frost sublimation (''Crocus date'') predates the mean depositional minima, as expected. These global-scale, volumetric measurements of the distribution of condensed CO_2 can be combined with measurements of the deposited column mass density derived from the Neutron Spectrometer on board Mars Odyssey to yield an estimate of the density of the seasonally exchanging material of 0.5 ± 0.1 g/cm^3. These constraints should be considered in models of the Martian climate system and volatile cycles. *INDEX TERMS:* 6225 Planetology: Solar System Objects: Mars; 5462 Planetology: Solid Surface Planets: Polar regions; 5464 Planetology: Solid Surface Planets: Remote sensing; 5494 Planetology: Solid Surface Planets: Instruments and techniques; 5445 Planetology: Solid Surface Planets: Meteorology (3346); *KEYWORDS:* CO_2, deposition, Mars

Citation: Aharonson, O., M. T. Zuber, D. E. Smith, G. A. Neumann, W. C. Feldman, and T. H. Prettyman (2004), Depth, distribution, and density of CO_2 deposition on Mars, *J. Geophys. Res.*, *109*, E05004, doi:10.1029/2003JE002223.

1. Introduction

[2] The dynamic role of volatiles on the surface of Mars has been a subject of long-standing interest. In the pre-Viking era, much of the debate was necessarily addressed by theoretical considerations. A particularly influential treatment was put forth by *Leighton and Murray* [1966], in which a simple model relying on solar energy balance was employed, and led to the conclusion that the most prominent volatile exchanging with the atmosphere over seasonal cycles is carbon dioxide. Their model suggested that due to this exchange, atmospheric CO_2 partial pressure is regulated by polar ice. While current thinking attributes a larger role to H_2O ice than the occasional thin polar coating this model predicted [*Jakosky and Haberle*, 1992], the essential CO_2 cycle described by *Leighton and Murray* [1996] appears to be largely correct [*Wood and Paige*, 1992].

[3] There are a number of observations indicating seasonal exchange of surface volatiles with the atmosphere on Mars. The growth and retreat of polar CO_2 frost is visible from Earth-based telescopes [*Martin et al.*, 1992] and from spacecraft in Mars orbit, both at visible wavelengths and in thermal IR properties of the surface [e.g., *Briggs et al.*, 1977; *James*, 1979; *Kieffer*, 1979; *Cantor et al.*, 1998; *James and Cantor*, 2001]. Measurements made by Viking's Mars Atmospheric Water Detector (MAWD) experiment were sensitive to atmospheric H_2O vapor abundance [*Farmer et al.*, 1977; *Jakosky and Farmer*, 1982]. Surface condensates and their transient nature were detected by the Viking landers [*Jones et al.*, 1979]. Recently, variations in gamma ray [*Kelly et al.*, 2003] and neutron fluxes [*Feldman et al.*, 2003; *Mitrofanov et al.*, 2003] have been used to infer integrated changes in CO_2 mass on the surface. The present study is motivated by data collected by the Mars Orbiter Laser Altimeter (MOLA) [*Zuber et al.*, 1992] on board Mars Global Surveyor [*Albee et al.*, 2001], affording the opportunity to not only detect the lateral distribution of volatiles [*Kieffer et al.*, 2000; *Titus et al.*, 2001], but also to constrain the variable volumes of

[1]Division of Geological and Planetary Sciences, California Institute of Technology, Pasadena, California, USA.
[2]Department of Earth, Atmospheric, and Planetary Sciences, Massachusetts Institute of Technology, Cambridge, Massachusetts, USA.
[3]Laboratory for Terrestrial Physics, NASA Goddard Space Flight Center, Greenbelt, Maryland, USA.
[4]Los Alamos National Laboratory, Los Alamos, New Mexico, USA.

0148-0227/04/2003JE002223$09.00

the reservoirs, and hence their densities. We build on the results of *Smith et al.* [2001a], who have estimated the latitudinal distribution of the deposits.

[4] The primary constituent of the Martian atmosphere is CO_2, and about a quarter of its mass has been estimated to exchange with the surface during a seasonal cycle [*James et al.*, 1992]. The cycle was first characterized quantitatively in a local sense during the Viking mission by measuring seasonal variations of atmospheric pressure at both landing sites [*Hess et al.*, 1979, 1980; *Leovy*, 1985; *Zurek et al.*, 1992]. A seasonal pressure change was also observed at the Pathfinder landing site over a small fraction (12%) of a Martian year [*Schofield et al.*, 1997]. No successful landing-site measurements have been made so far in the southern highlands. Radiative balance calculations [*Paige and Ingersoll*, 1985; *Paige*, 1992; *Paige and Wood*, 1992] and general circulation models (GCMs) [*Haberle et al.*, 1993] constrained by Viking lander pressure data estimate the mass of the condensed deposits to be consistent with a maximum amplitude at the poles of about 1 m of solid CO_2 ice. While both the north and south seasonal frost is composed of CO_2, temperatures during summer seasons indicate that the residual cap in the north is composed of H_2O [*Kieffer et al.*, 1976], while the much smaller residual ice in the south is covered with CO_2 [*Kieffer*, 1979]. The south pole CO_2 deposits may be underlain with H_2O ice, an idea supported by atmospheric water vapor seen by Viking in some years [*Jakosky and Haberle*, 1990], by morphological [*Byrne and Ingersoll*, 2003] and thermal [*Titus et al.*, 2003] observations, by constraints based on the thermal conductivity of CO_2 [*Mellon*, 1996], and by laboratory measurements on the rheology of CO_2 [*Nye et al.*, 2000] which indicate a CO_2 ice cap would flow away on geologically short timescales. The differences between the northern and southern frost deposition and sublimation (and perhaps ultimately, cap composition) is traditionally attributed to several factors [*Thomas et al.*, 1992]. The Viking orbiter result that 75 ± 12 g/cm^2 of CO_2 were deposited in the north, and 110 ± 7 g/cm^2 in the south [*Paige and Ingersoll*, 1985] during one year of observations, is attributed to the longer winter season in the south. The relatively darker albedo of north polar cap may be due to higher dust concentration [*Paige and Ingersoll*, 1985] that also leads to enhanced sublimation rates. Recently, *Richardson and Wilson* [2002] suggested that a topographically forced asymmetry in the Hadley cell circulation controls global transport of H_2O. In their calculation, the topography creates a preference for the active formation of polar layered deposits in the north, independent of the perihelion timing.

[5] Optical and spectral techniques are sensitive to the spatial distribution of surface frost, but as they observe only the top surface are not useful in estimating volumes involved in the exchange, nor the rates of deposition and sublimation. In order to quantitatively characterize the spatial and temporal pattern of volatile exchange, we elaborate on a technique first employed by *Smith et al.* [2001a]. By examining averages of a large number of topographic measurements collected by the MOLA, *Smith et al.* [2001a] showed that the zonal pattern of deposition and sublimation of CO_2 can be determined. In their first approach, reference surfaces were fit to all measurements in narrow latitude annuli, and the time dependent variations about those mean surfaces were examined. In their second approach, height measurements from pairs of tracks that cross on the surface were interpolated and differenced, forming a set of crossover residuals. These residuals were then examined as a function of time and latitude. The initial studies averaged over longitude to maximize signal and minimize noise in order to isolate the expected small signal. In this follow-up study we now attempt to extract the elevation change pattern also as a function of longitude, and have focused on the crossover approach.

2. Data Quality and Processing

[6] The accurate recovery of changes in elevation depends upon the quality of the laser-derived range measurements from which the residuals are derived. We therefore briefly review the error estimates affecting the crossover measurements. Estimations of surface height are prone to error, introduced both by the range measurement itself, as well as from imperfect knowledge of the position and orientation of the spacecraft.

[7] The range from the spacecraft to surface is obtained from the round-trip time-of-flight of a laser pulse arriving back at the MOLA detector, and hence includes timing errors and errors due to the receiver's response. The precision of the timing measurement is limited by the clock accuracy of $\sim$2.5 ns, corresponding to 37.5 cm, but suffers from systematic drifts in the clock frequency. These daily variations are estimated and calibrated to better than 1 part in 10^8 [*Neumann et al.*, 2001; *Smith et al.*, 2001b]. Modeling of the instrument [*Abshire et al.*, 2000; *Gardner*, 1992] allows a correction to be applied, accounting for variability in shape and strength of return pulses that affects the instrument's triggering time. This correction, referred to as "range walk", is typically 1–3 m in amplitude, and has an uncertainty of approximately 30 cm [*Neumann et al.*, 2001].

[8] The position of the spacecraft relative to Mars' center of mass is obtained from spacecraft tracking solutions [*Lemoine et al.*, 2001]. The deduced gravitational field expressed in terms of the static equipotential height ("areoid"), as well as the time dependent position and attitude of the spacecraft information ("orbits"), are used to determine the topographic height.

[9] In the final step of the processing, the elevation measurements themselves are used to improve the orbital solutions. The elevations of locations where a pair of ground-tracks of measurements intersect (Figure 1), are interpolated and differenced to form a set of "crossover residuals". These residuals may include both real surface height changes, as well as systematic errors in the orbital position that arise, for example, from imprecise knowledge of the gravity field.

[10] To reduce the effect of systematic error sources, the set of raw crossover residuals was adjusted by deriving a correction for each track such that the $\sim$9 million residuals equatorward of 57° latitude or occurring within the same discrete 15-day period were minimized, since no change is expected for these measurements. This minimization is carried out by least-squares fitting of orbital adjustment

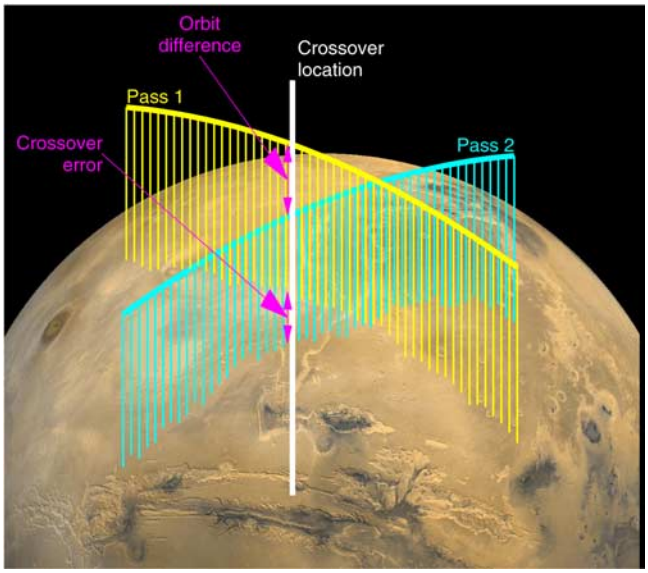

Figure 1. Crossover errors are determined by interpolation of crossing ground tracks. In the cartoon, the ground location where two passes cross is indicated with a white bar which intersects pass 1 at a higher altitude than pass 2. Removal of systematic orbit differences results in the change in surface height.

parameters, using three-dimensional, smooth (polynomial), functions of time [*Rowlands et al.*, 1999; *Neumann et al.*, 2001; *Smith et al.*, 2001b], with 4 parameters controlling the once-per-rev (orbit) component, and 4 additional parameters for the twice-per-rev component in each dimension. In the preferred model, the fitting problem is over-constrained, as there are roughly 200 times more measurements than fitted parameters. Applying these adjustments, and recomputing the crossover residuals, reduces their root-mean-square from the initial value 8.3 m, down to 1.8 m [*Neumann et al.*, 2001]. The correction was then applied to all tracks and the entire set of ~66 million residuals recomputed. To minimize random errors, residuals resulting from less reliable measurements were excluded. These include measurements obtained on slopes greater than 10°, off-nadir observations, and residuals >10 m [*Smith et al.*, 2001a]. This criterion eliminates data collected in latitudes 87.3° to the poles (owing to the spacecraft's inclination angle of 92.7°), as these off-nadir polar observations are characterized by significant errors due to range walk.

[11] Several variations on the above scheme were conducted in order to test the minimization procedure. These included shortening the temporal bins within which crossovers were minimized to 7 days, restricting the minimized residuals' latitudes to equatorward of 45°, and fitting only periods of once-per-rev. These tests all showed the same qualitative behavior: while the variance of the data increased in places, the pattern of residuals near the pole stayed the same, within about 10 cm.

3. Time-Dependent Topography

[12] The intersections of MOLA ground-tracks (i.e., crossovers, as represented in Figure 1) provide a useful means of determining changes in the topography occurring during the time interval between the measurements. The amplitude of any seasonal change is expected to be small in comparison to the local topography, and reducing systematic and random errors as described above is crucial. By averaging a large number of observations it is possible to isolate temporal height changes from random errors at an accuracy of better than 10 cm [*Smith et al.*, 2001a]. However, systematic errors which may be correlated with surface properties such as albedo and roughness remain. In order to treat the data uniformly when forming averages, each crossover residual is counted twice: once with the time tag of the later track, and again, with the time tag of the earlier track (and an opposite sign).

[13] The global redistribution of CO_2 on the surface can be seen by averaging the crossover residuals δz over all longitudes, as a function of latitude and season. Figure 2 shows the seasonal dependence of deposition for a selected high-latitude 0.5° annulus, centered on 86°N and 86°S, as a function of solar longitude L_s (defined such that $L_s = 0°$ at northern vernal equinox, and $L_s = 90°$ at northern summer solstice). Several features in the plot are in agreement with *Smith et al.* [2001a]: the amplitudes of residuals are seen to be maximum in both hemispheres during their respective late winters, just before $L_s = 0°$ in the north, and $L_s = 180°$ in the south. The amplitude of the fluctuation peak to peak in this latitude band is ~2.5 m in the south, somewhat larger than ~1.5 m amplitude in the north. This component of the signal is generally consistent with predictions by global circulation models of Mars' climate. The asymmetry, not seen in *Smith et al.* [2001b], is due to the eccentric orbit of Mars resulting in a greater solar distance and longer duration of the winter season in the south. Assuming that the error source is Gaussian (as verified by examining the

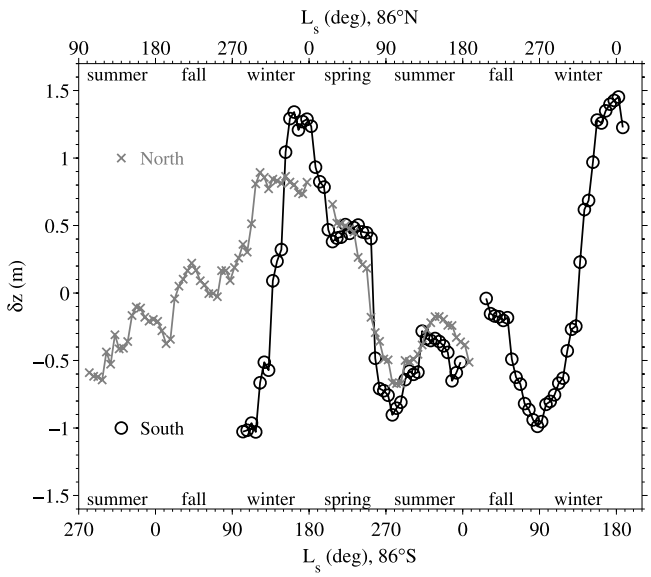

Figure 2. Average accumulation as a function of the seasonal parameter L_s, averaged over longitude in a 0.5° annulus at 86° north (crosses) and south (circles) latitude. The data gap following $L_s \sim 0°$ is due to the instrument being turned off during superior conjunction. An empirical estimate of the error in these averages is ~15 cm, but the formal values of σ_m are substantially smaller.

residuals near the equator), the formal error associated with mean residuals, σ_m, is given by

$$\sigma_m = \frac{\sigma}{\sqrt{N}}, \quad (1)$$

where σ is the standard deviation of the data and N is the number of measurements. The magnitude of σ_m is small, typically less than 1 cm due to the large number of crossovers in that latitude used in forming the means. However, this formal error is deceptive because in practice, unmodeled systematic errors are not negligible. An alternative way to estimate the errors empirically is to examine residuals in latitudes where no seasonal component is expected but no residual minimization was applied. This standard deviation of the mean is typically 15 cm, and represents a more realistic estimate of the error.

[14] The removal of material by sublimation progresses similarly at latitude 86° in both hemispheres (between L_s = 0–90° in the north, and L_s = 180–270° in the south), as shown in Figure 2. However, the build up in the south, starting at L_s ~115°, is more abrupt, with almost all the change in elevation occurring during only about 45° in L_s. This relatively late, abrupt buildup is repeated in the second mapping year, and if real, this difference awaits explanation. One possibility is that the accumulation seen in mid- to late-southern winter consists of low density deposits that account for the elevation difference, while earlier deposits of higher density are not easily detected. If CO_2 snow accumulation on Mars has some analogy with H_2O accumulation on Earth it would be expected that the density of deposits would increase over the course of the winter season due to settling, compaction, and annealing [*Eluszkiewicz*, 1993; *Eluszkiewicz and Titus*, 2003]. This would, however, be opposite to the effect noted above. An alternate idea is that the nature of the condensation in space and time has relevance. If some condensation occurs out of the atmosphere as snow and some at the surface as frost, and if one mechanism is favored at different times of winter, then the density of surface deposits would vary seasonally. Further work is needed to address the style of condensation and its relationship to CO_2 deposits.

[15] An additional surprising aspect of the plot is seen in the increased "off-season" accumulation, which begins to build up in mid summer in both hemispheres. During these times, an unexpected enhancement in deposition occurs at high latitudes, which decays again before the onset of winter. *Smith et al.* [2001a] suggest that in the north the decay may be related to the warming of the atmosphere by regional dust storms observed near L_s = 240°. The signals are seen in both crossover and profile analyses of the MOLA data [*Smith et al.*, 2001a], and occur in both years. However, it is not yet possible to conclude they are a consequence of meteorological phenomena as unmodeled aspects of the response of the MOLA receiver may contribute to systematic errors. In particular, seasonal brightening of the polar caps may lead to residual errors in the range walk correction. Significant analysis of the impulse response of the MOLA receiver has been performed [*Abshire et al.*, 2000; *Smith et al.*, 2001b; *Neumann et al.*, 2003] and corrections have been applied to the data included in the present analysis, but efforts to better understand the response of the MOLA receiver, especially to changes in surface reflectivity, are ongoing [*Neumann et al.*, 2002]. At present, these systematics are estimated to produce errors in pulse timing of less than ~2.4 ns, corresponding to ~35 cm in elevation. The late summer elevation rise seen in both polar regions is not associated with dramatic changes in albedo at 1.064 micron as determined by passive measurements by the MOLA instrument, so it appears unlikely that this instrumental effect is responsible. Alternatively, one, or several of a number of factors may be responsible for accumulation not seen in GCMs where these factors are ignored or approximated. Local shadowing by topography may contribute to enhanced accumulation. In polar regions such shadowing can be either nearly permanent, or merely sufficiently long in duration to alter the expected deposition/sublimation balance. Squalls, or local storms, may also contribute to the signal, but constraining their relative roles awaits further advances in mesoscale modeling [e.g., *Rafkin et al.*, 2001; *Toigo and Richardson*, 2002]. However, as evidence for these accumulations has thus far not been seen in other data, such as that collected by the Neutron Spectrometer, this result should be considered suspect.

[16] Crossover residuals were sorted into spatial bins in latitude-longitude. Since MGS is in an approximately polar orbit, the number of elevation measurements in each bin is approximately uniform. However, since the number of crossovers increases as the square of the number of orbits, regular grids have cells with more crossovers near the pole, improving the statistical quality of high-latitude measurements with respect to low-latitudes.

[17] In each spatial bin, we sorted the data in time (L_s), and applied a least-squares fit (using the Levenberg-Marquardt method, implemented by [*Press et al.*, 1992]), to a function of the form

$$\delta z(L_s) = -\sum_{n=1}^{n_{\max}} A_n \cos(nL_s - D_n). \quad (2)$$

Initially we examine the first two terms, corresponding to the seasonal n = 1 and semiannual n = 2 variations. The coefficients A_n are the amplitudes, and D_n are the phases of the cosines' minima. If, for example, the accumulation was minimum on the last day of summer, the phase D_1 would be 180° in the north and 0° in the south.

[18] Figures 3 and 4 show a summary of the north and south polar data. The maps shown in the left column correspond to (a) the annual term amplitude A_1, (b) phase D_1, and (c) the number of crossovers in each cell N. Panel (d) shows a simplified geologic map [*Tanaka and Scott*, 1987] of the region, and (e) is the topography superimposed on shaded relief. The date shown in (f) will be discussed later.

[19] In the north (Figure 3), the amplitude of the first harmonic A_1 is seen to increase with latitude, and while there may be a weak correlation, there is no abrupt change as the polar cap boundary is encountered. Locally, the amplitude can be as high as 1 m (2 m peak to peak), but more typically it is 0.4–0.6 m on the cap. The phase of the first harmonic D_1 ~135° remains constant on the ice cap, and is only slightly more variable off the cap. This consistency in space is taken as an indication of the robustness of the fit. In the region between 70–80°N and 180–270°E the amplitude is reduced, and as expected, the phase is more variable.

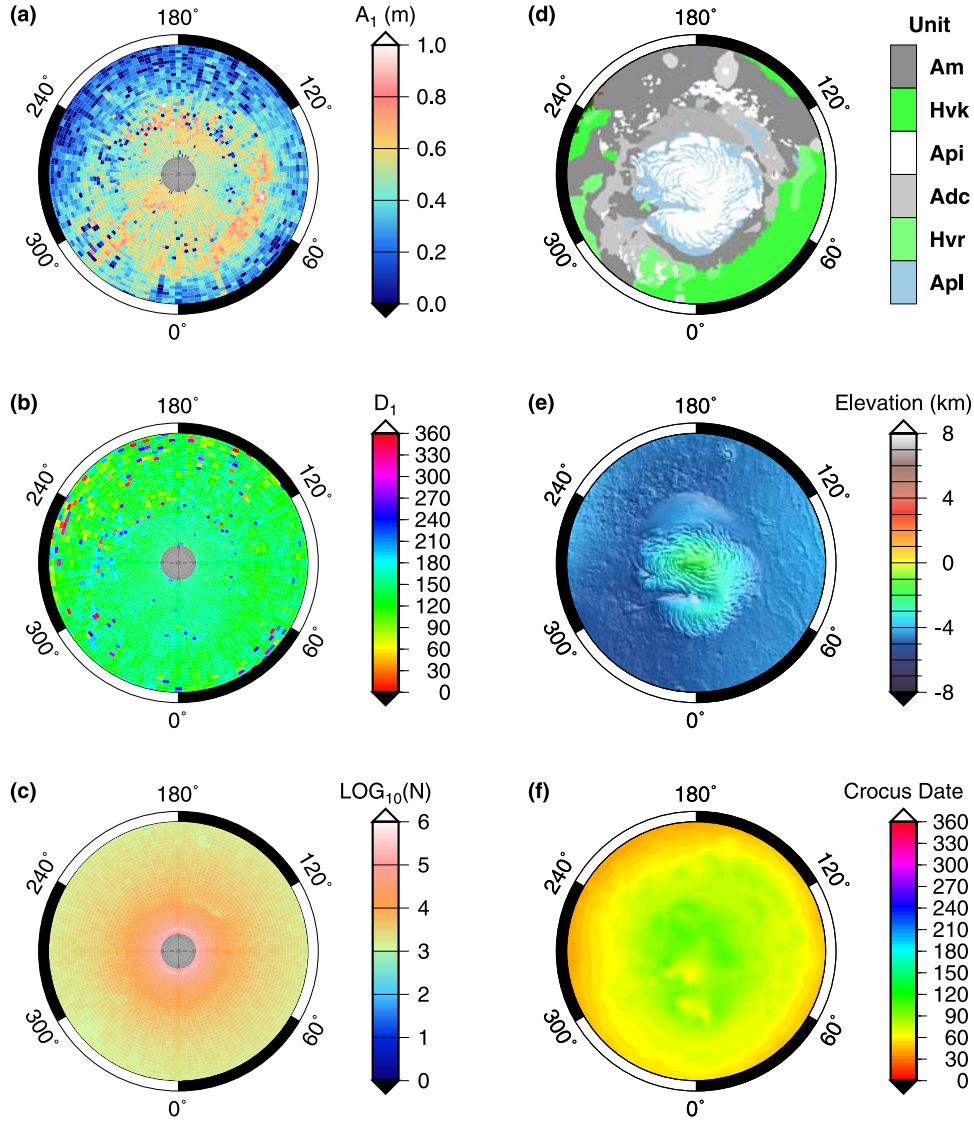

Figure 3. North Pole. Panels correspond to maps of (left column) annual sinusoid amplitude, phase, the number of crossovers used, (right column) geology, topography, and crocus date. All maps are in a polar stereographic projection, from 70°N to the pole, with bins of size 3° in longitude and 0.5° in latitude.

[20] In the south (Figure 4), the amplitude A_1 is strongly correlated with the residual cap (unit Api). Further modeling is required in order to determine the cause of this strong correlation, but one likely possibility is that the enhanced accumulation is related to the persistent colder temperatures and higher albedo on that unit. The boundary of the layered terrain (unit Apl) does not appear to have a signature in the amplitude pattern. The phase of the first harmonic in the high southern latitudes is D_1 ~355°. Relatively static areas are again observed. The non-axisymmetric pattern highlights the importance of spatially resolving the mean residuals, as there is at least 50% variation in the amplitude within latitude bands.

[21] For both the north and south maps, we have more confidence in the amplitude measurement when the phase is consistent for nearby areas. When the phase is "noisy", the amplitude measurement is suspect. Furthermore, as indicated by N, the highest latitude bins have ~3 orders of magnitude more crossovers than the ones at 70°, and are therefore statistically better defined.

[22] Figures 5, 6, and 7 show detailed maps of the fitted parameters for the north, south and equatorial regions, as well as the respective formal error estimates. As expected from the distribution of N, the estimates improve near the poles, so that the amplitude of the fitting error drops from ~10 cm in equatorial regions to <2 cm near the pole, and the phase changes from being unconstrained in latitudes equatorward of 65°, to having an error of <3° near the poles. Here again it should be emphasized that the formal fitting errors do not include non-negligible systematics.

[23] In the north, while the annual term is only weakly correlated with the cap deposits, the semiannual term (especially the phase D_2) is highly correlated with local geology. In particular, the consistency of the phase D_2 of the semiannual component on the cap surface suggests that this dynamical behavior is robust and is maintained from year to

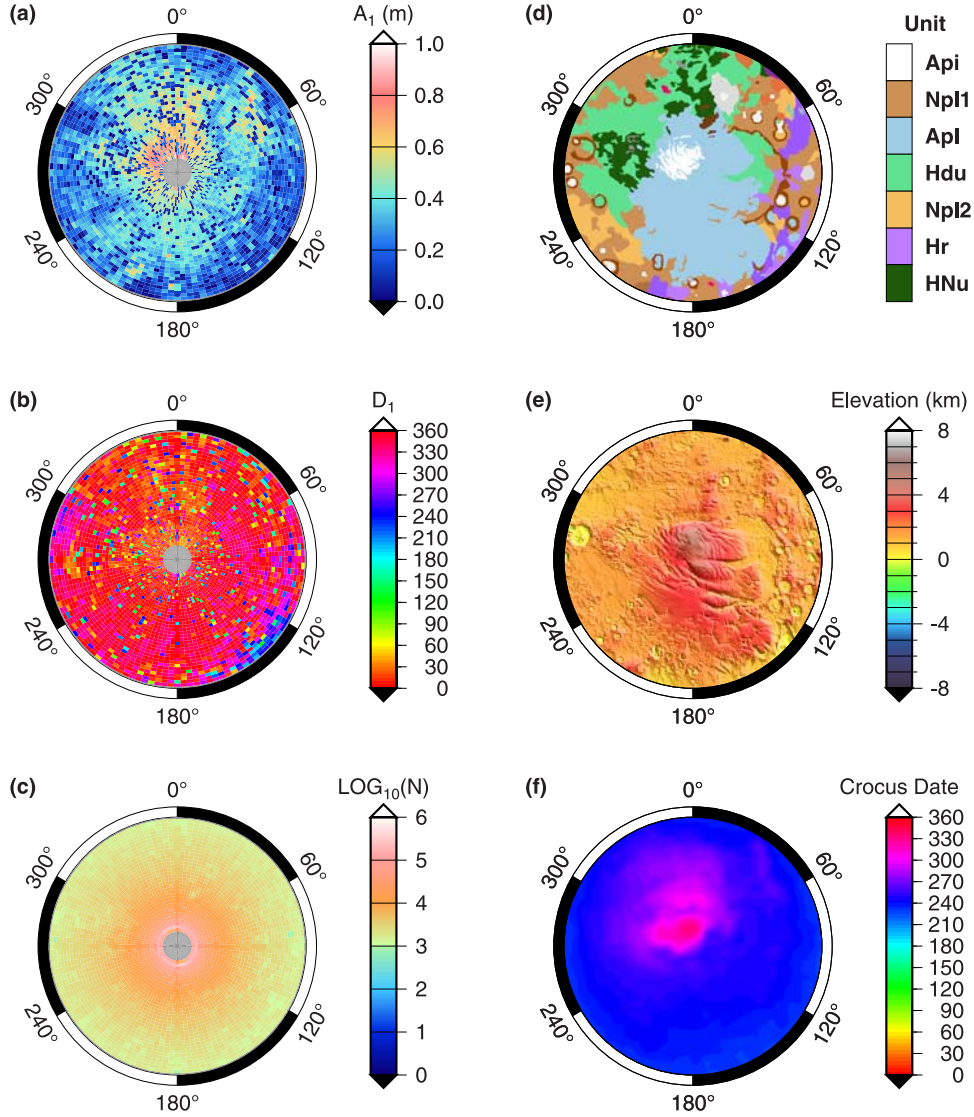

Figure 4. South Pole. Panels correspond to maps of (left column) annual sinusoid amplitude, phase, the number of crossovers used, (right column) geology, topography, and crocus date. Maps are in a polar stereographic projection, from 70°S to the pole, with bins of size 3° in longitude and 0.5° in latitude.

year. There are a number of possible causes that could play a role in explaining this relationship, and they include effects of elevation, albedo, and exposure to solar insolation. The amplitude of this component is especially high on the dune covered Olympia Planitia (82°N, 166°E), where sand and dust transport may be important and the topography is strongly aliased with MOLA measurements. In the south, the semiannual term is present, but surface geology appears to be less important. The equatorial region shows no consistent phase and a very noisy amplitude distribution. Figure 7 shows the transition to greater amplitude and more consistent phase with increasing latitude. Poleward of 65° latitude in both hemispheres, the variability of D_1 drops dramatically.

4. Comparison With Thermal Crocus Date

[24] As shown, the volumetric redistribution of CO_2 on the surface can be decomposed into harmonics in time, and the phases of these harmonics examined. Thermal observations can be used as an independent approach to describe the temporal retreat of surficial CO_2, using data from the Thermal Emission Spectrometer [*Christensen et al.*, 1992] on board MGS. In order to avoid absorption bands in the atmosphere, we follow *Kieffer et al.* [2000], and use the 30 μm band to define the temperature T_{30}. This temperature is sensitive to the warming of the surface that occurs when CO_2 sublimates away; while CO_2 is present, surface temperatures are buffered at T_{30} = 148 K. After CO_2 has completely sublimated the surface warms to a new equilibrium temperature, typically more than 10 degrees higher. The surface was divided into a regular grid, and an arc-tangent function used to fit the temperature increase in each cell, with the form

$$T_{30}(L_s) = T_0 + \frac{\Delta T}{\pi} \arctan\left(\frac{L_s - C}{\varphi}\right), \quad (3)$$

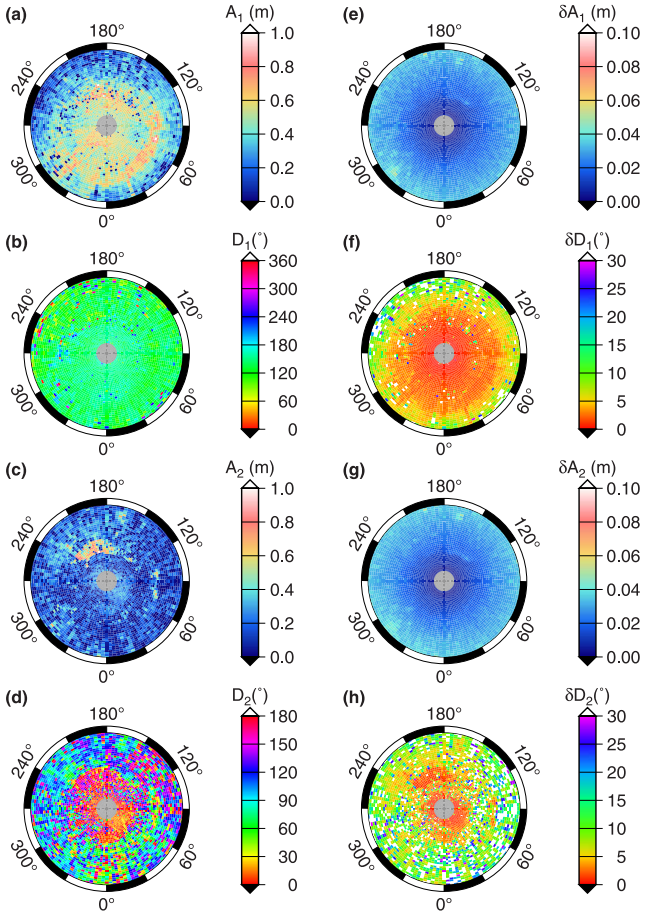

Figure 5. North Pole. Panels correspond to maps of (left column) amplitude and phase of the annual, and semiannual topography change, as well as (right column) the 1-σ error estimate in each quantity. Map format is the same as in Figure 3.

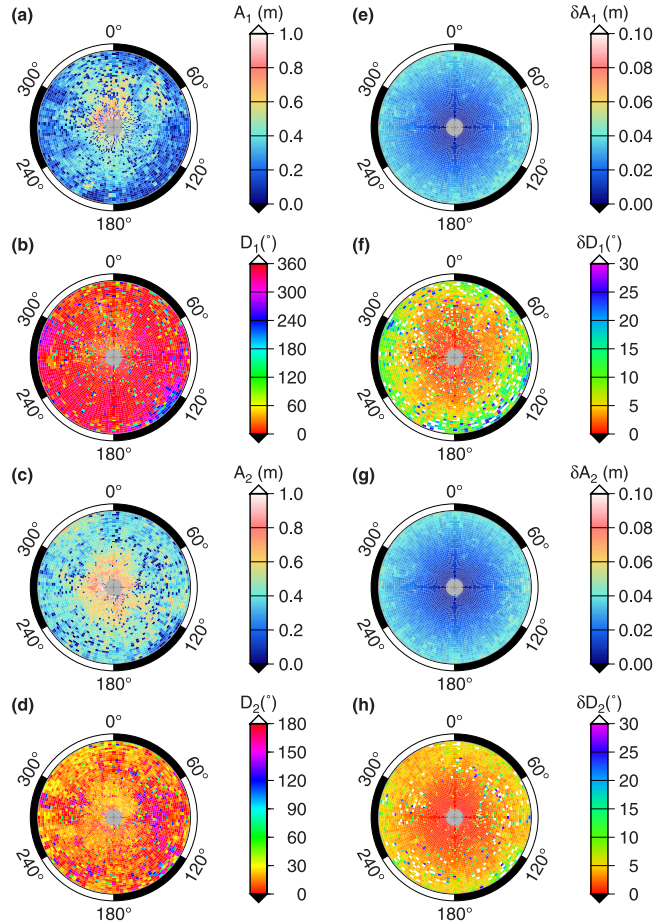

Figure 6. South Pole. Panels correspond to maps of (left column) amplitude and phase of the annual, and semiannual topography change, as well as (right column) the 1-σ error estimate in each quantity. Map format is the same as in Figure 4.

where L_s is the season, T_0 is the brightness temperature at the date C (in units of L_s), and and ΔT are the characteristic time and temperature increase for the transition from CO_2 frost to soil. As defined by *Kieffer et al.* [2000], C corresponds to the date at which Cap Recession Observations indicate CO_2 has Ultimately Sublimated (CROCUS), and is thus termed the "crocus date". Those authors point out the coincidence that crocuses are some of the first flowers that can be seen just after the last snow-melt in early spring.

[25] Maps of crocus date from *Kieffer et al.* [2000], are shown in Figures 3f and 4f. The north polar maps show that the crocus date C occurs at a similar time or earlier than the first phase D_1. The retreat of the frost covered area is seen to occur relatively uniformly, at a rate of approximately 3–3.5° of L_s per one degree of latitude. The crocus date approaches the value of ~95° near the pole, similar to D_1. In contrast, the behavior at the southern polar cap is again seen to be less symmetric in longitude. In areas where CO_2 ice is present throughout the year, the fits often fail to converge and C is meaningless. Off the cap, C changes from ~240° to 300°, again earlier than is seen in D_1. The difference between C and D_1 at both poles, is likely a consequence of the fact that the deposition is not truly sinusoidal. The crocus date is sensitive to the precise day that the ice disappeared, while D_1 measures the phase of the cycle as a whole. While the value of C is consistently smaller than D_1, the fluctuations in the two quantities are not independent in space.

5. Comparison With Mass Estimates From Gravity, GCMS, and Neutron Flux

[26] We compare our observations to a prediction from the Ames General Circulation Model (GCM), described in detail by *Pollack et al.* [1990], and reported on by *Smith et al.* [1999]. This model features a resolution of 7.5° in latitude, 9° in longitude, and 0.5–5 km vertically. The model employs conservation equations of mass, energy, and momentum, as well as a hydrostatic condition, radiative transport associated with dust loading, and a CO_2 ideal gas law. The seasonal cycle of CO_2 as simulated by the GCM is summarized in Figure 2 of *Smith et al.* [1999].

[27] Surface CO_2 ice is predicted to exchange with the atmosphere in the north and south with an opposite annual phase. The locations of the maxima peaks are better defined than the broader minima, and they occur near $L_s = 0°$ in the north and $L_s = 150°$ in the south. However, these peaks are

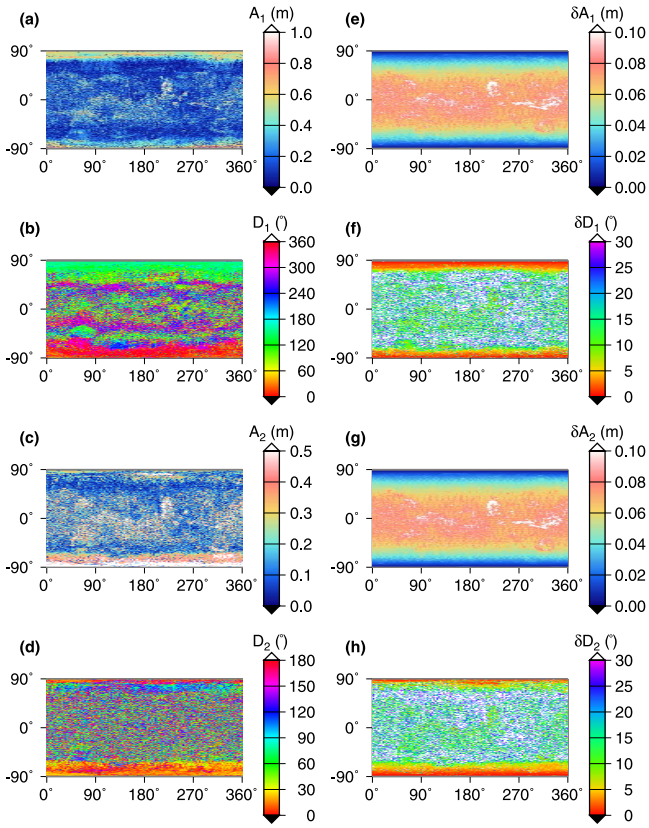

Figure 7. Equatorial region. Panels correspond to maps of (left column) amplitude and phase of the annual, and semiannual topography change, as well as (right column) the 1-σ error estimate in each quantity. Maps are in a simple cylindrical projection, with bins of size 3° in longitude and 0.5° in latitude.

shifted with respect to a mean sinusoidal component of the variation, which more closely agree with the observed phase D_1 in both hemispheres.

[28] The amplitudes of the surface exchange in the north and south do not balance, resulting in a net semiannual oscillation in the total surface mass (balanced by atmospheric storage). In the model, the amplitude of the oscillation in the south is ~65% greater than in the north, owing to the longer cold season. The material implicated in the exchange perturbs the gravitational field of Mars in a time-dependent manner. This change is observable by tracking the orbiting spacecraft and modeling its accelerations. Analysis by *Smith et al.* [2001a] suggests that the estimates from the GCM, and the gravitational and topographic perturbations are generally consistent with each other if the density of the material is 0.91 ± 0.23 g/cm^3, with the uncertainty in the estimate dominated by that of the time-varying gravity signal.

[29] An additional means of constraining the mass exchanged is possible by analysis of the enhancement of epithermal neutrons which form an equilibrium flux distribution in both the H_2O substrate and CO_2 cover. Observations by the Neutron Spectrometer [*Feldman et al.*, 2003] and High Energy Neutron Detector [*Mitrofanov et al.*, 2003] on board Mars Odyssey have been used to derive this time-dependent column mass abundance. Here, we employ the epithermal neutron fluxes used in *Feldman et al.* [2003], which are sensitive indicators of mass changes. In Figure 8 a comparison between the MOLA-derived heights δz from this study, the neutron-derived column density Σ, and a modified GCM prediction [*Haberle et al.*, 1993; *Pollack et al.*, 1993] is shown. The zero level of the height data was chosen such that the mean height residuals are zero. The relative scaling of the vertical axes is arbitrary. The data from the Neutron Spectrometer was obtained from the region poleward of 85°, so MOLA data was integrated from 85°N up to 87°N, above which only imprecise off-nadir residuals are available. This latitude band includes only a fraction of the total mass deposited, but is used as representative of the high-latitude deposits.

[30] The neutron data is seen to agree well in phase and relative amplitude with the AMES GCM 6 model, which was adjusted using the measured attenuation of the hydrogen gamma ray line [*Feldman et al.*, 2003]. Both correspond closely in the timing of the decline to that measured from MOLA. In particular these three data sets all predict the cap should be reduced by about 50% at about $L_s = 70°$. Additional data and analysis from neutron spectroscopy will allow a comparison of the growth phase of the curve, as well as of the period of maximal accumulation that is seen to be broad in MOLA residuals. Figure 9 plots the neutron-derived CO_2 column density against the MOLA-derived height change. The slope of a line fitting this data is an estimate of the mass density of the deposit, robust in that it represents a fit to all the points simultaneously. The slope of the best fit line is 0.5 ± 0.1 g/cm^3. Here the error estimate is based on the ratio (20%) of the scatter of the observations at latitudes where crossover residuals are expected to exhibit a seasonal component to that at latitudes where no seasonal change is expected. As a conservative estimate, this approach assumes that errors are systematic; if errors were purely random the uncertainty in the slope would be considerably smaller.

[31] The best-fit density is lower than estimated previously [*Smith et al.*, 2001a; *Yoder et al.*, 2003] from time-varying topography and gravity, and implies a high porosity (about 2/3 void spaces), but is in accord with another recent study from neutron spectrometry and MOLA [*Feldman et al.*, 2003]. The lower density supports the notion that a substantial part of the seasonal mass precipitates in the form of snowfall [*Forget et al.*, 1998], since by analogy to terrestrial water ice, such deposits are expected to be of lower density than surface frost. Subsequent densification of these deposits is possible [*Eluszkiewicz*, 1993; *Eluszkiewicz and Titus*, 2003], and could explain some of the deviations from a straight line, as well as spectral constraints on grain size distribution [*Kieffer and Titus*, 2001]. However, at present the height data is of insufficient quality to require such effects. Finally, the comparison of mass and volume here is restricted to latitudes 85–87°N and roughly to the northern spring season. The results at lower and at southern latitudes may be different.

6. Summary

[32] Our results demonstrate that the large number of MOLA elevation measurements can be effectively corrected, averaged and fitted, to yield sensitive measurements

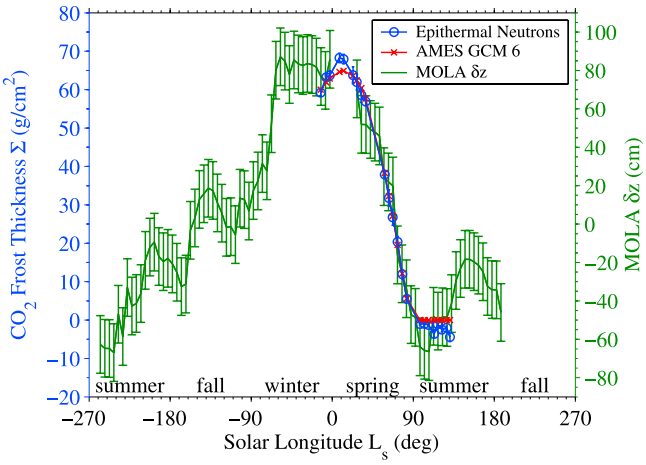

Figure 8. MOLA-derived height changes for the north polar cap, averaged in the latitude range 85–87°N (solid line, right axis), shown together with estimates of the column surface mass density of the seasonal deposits Σ derived from epithermal neutron flux (circles, left axis), and a GCM (crosses, left axis). Elevation data are shown with approximate 15 cm error bars (see text for estimation). Calibration of the neutron data results is a few small negative values for the frost thickness which are not physical [*Feldman et al.*, 2003]. The ratio of the scales of the vertical axes is 0.5 gm/cm^3. The elevation and mass data were obtained during different Mars years.

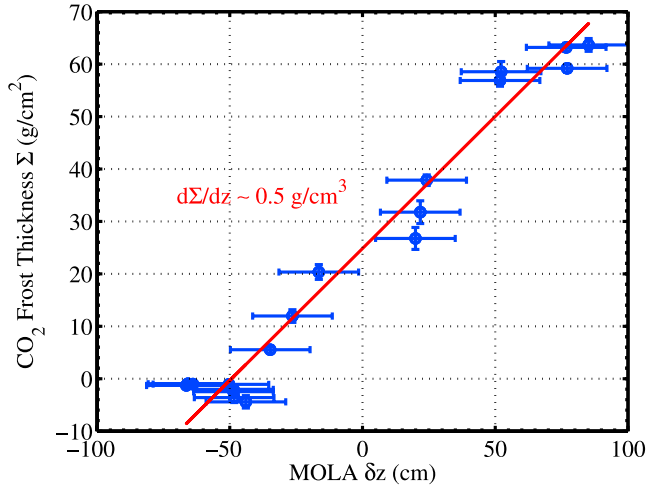

Figure 9. Integrated north pole CO_2 column mass plotted from epithermal neutron measurements plotted against MOLA height changes using observations poleward of 85°N, as shown in Figure 8. Each point represents an L_s interval of ~5°.

of the changes in polar surface height as a function of both latitude and longitude over the Martian seasonal cycles. Accumulation is expected and observed to be maximum in late winter, and at high latitudes at both hemispheres. More perplexing are apparent deposition/sublimation episodes during warmer seasons which may be related to unmodeled instrument response. In order to resolve the dependence of the pattern on longitude and time, a harmonic decomposition of the signal was carried out locally. The annual component of the signal is strongly correlated with the residual south polar cap deposits, and weakly with the north polar cap. In the north, the second harmonic (semiannual) component correlates strongly with geologic units. The phases of the annual cycles are in agreement with thermal observations of the timing of the annual disappearance of CO_2 frost from the surface ("crocus date") at the high latitudes, as well as with predictions from global circulation models. At lower latitudes, frost sublimation predates the fitted minima of the annual cycle. Consideration of the height changes averaged over the north polar cap together with mass change estimates from a GCM and neutron flux measurements, yields an estimate for the mean density of the seasonal deposits of 0.5 g/cm^3. This estimate is lower than that previously derived from joint analysis of gravity and topography [*Smith et al.*, 2001b; *Yoder et al.*, 2003]. The density difference arises partly from a higher peak-to-peak height change resolved here, and partly from a column density that is most compatible with the lower end of the gravity estimates (~3 × 10^{15} kg for models in which the cap thickness is linear with latitude). These mass estimates can differ due to factors including a more restricted temporal and spatial analysis of the neutron data than of the global gravity field, as well as uncertainties in the time-dependence of the gravity.

[33] These results provide constraints that should be incorporated in future models of the Martian climate system and volatile cycles. In addition, the geographic correlations of the amplitude and phase of the signal with surface features, supports both the interpretation of the data as depositional in origin, and the utility of crossovers for analyses of subtle temporal changes of planetary elevation.

[34] **Acknowledgments.** We acknowledge helpful discussions with Hugh Kieffer and suggestions by two anonymous reviewers. This work was supported by the NASA Mars Data Analysis Program and Mars Exploration Program.

References

Abshire, J. B., X. Sun, and R. S. Afzal (2000), Mars Orbiter Laser Altimeter: Receiver model and performance analysis, *Appl. Opt.*, *39*, 2440–2460.

Albee, A. L., R. E. Arvidson, F. Palluconi, and T. Thorpe (2001), Overview of the Mars Global Surveyor mission, *J. Geophys. Res.*, *106*, 23,291–23,316.

Briggs, G., K. Klaasen, T. Thorpe, J. Wellman, and W. Baum (1977), Martian dynamical phenomena during June–November 1976: Viking orbiter imaging results, *J. Geophys. Res.*, *82*, 4121–4149.

Byrne, S., and A. P. Ingersoll (2003), A sublimation model for Martian south polar ice features, *Science*, *299*, 1051–1053.

Cantor, B. A., M. J. Wolff, P. B. James, and E. Higgs (1998), Regression of Martian north polar cap: 1990–1997 Hubble Space Telescope observations, *Icarus*, *136*, 175–191.

Christensen, P. R., et al. (1992), Thermal Emission Spectrometer experiment: Mars Observer mission, *J. Geophys. Res.*, *97*, 7719–7734.

Eluszkiewicz, J. (1993), On the microphysical state of the Martian seasonal caps, *Icarus*, *103*, 43–48.

Eluszkiewicz, J., and T. N. Titus (2003), A microphysically-based approach to inferring porosity, grain size, and dust abundance in the seasonal caps from atmospherically-corrected TES spectra, paper presented at Third International Conference on Mars Polar Science and Exploration, Lunar and Planet. Inst., Alberta, Canada.

Farmer, C. B., D. W. Davies, A. L. Holland, D. D. Laporte, and P. E. Doms (1977), Mars: Water vapor observations from the Viking orbiters, *J. Geophys. Res.*, *82*, 4225–4248.

Feldman, W. C., et al. (2003), CO_2 frost cap thickness on Mars during northern winter and spring, *J. Geophys. Res.*, *108*(E9), 5103, doi:10.1029/2003JE002101.

Forget, F., F. Hourdin, and O. Talagrand (1998), CO_2 snowfall on Mars: Simulation with a general circulation model, *Icarus*, *131*, 302–316.
Gardner, C. S. (1992), Ranging performance of satellite laser altimeters, *IEEE Trans. Geosci. Remote Sens.*, *30*, 1061–1072.
Haberle, R. M., J. B. Pollack, J. R. Barnes, R. W. Zurek, C. B. Leovy, J. R. Murphy, H. Lee, and J. Schaeffer (1993), Mars atmosphere dynamics as simulated by the NASA Ames General Circulation Model: 1. The zonal mean circulation, *J. Geophys. Res.*, *98*, 3093–3123.
Hess, S. L., R. M. Henry, and J. E. Tillman (1979), The seasonal variation of atmospheric pressure on Mars as affected by the south polar cap, *J. Geophys. Res.*, *84*, 2923–2927.
Hess, S. L., J. A. Ryan, J. E. Tillman, R. M. Henry, and C. B. Leovy (1980), The annual cycle of pressure on Mars measured by Viking landers 1 and 2, *Geophys. Res. Lett.*, *7*, 197–200.
Jakosky, B. M., and C. B. Farmer (1982), The seasonal and global behavior of water vapor in the Mars atmosphere: Complete global results of the Viking atmospheric water detector experiment, *J. Geophys. Res.*, *87*, 2999–3019.
Jakosky, B. M., and R. M. Haberle (1990), Year-to-year instability of the Mars south polar cap, *J. Geophys. Res.*, *95*, 1359–1365.
Jakosky, B. M., and R. M. Haberle (1992), The seasonal behavior of water on Mars, in *Mars*, edited by H. H. Kieffer et al., pp. 969–1016, Univ. of Ariz. Press, Tucson.
James, P. B. (1979), Recession of Martian north polar cap: 1977–1978 Viking observations, *J. Geophys. Res.*, *84*, 8332–8334.
James, P. B., and B. A. Cantor (2001), Martian north polar cap recession: 2000 Mars Orbiter Camera observations, *Icarus*, *154*, 131–144.
James, P. B., H. H. Kieffer, and D. A. Paige (1992), The seasonal cycle of carbon dioxide on Mars, in *Mars*, edited by H. H. Kieffer et al., pp. 934–968, Univ. of Ariz. Press, Tucson.
Jones, K. L., R. E. Arvidson, E. A. Guinness, S. L. Bragg, S. D. Wall, C. E. Carlston, and D. G. Pidek (1979), One Mars year—Viking lander imaging observations, *Science*, *204*, 799–806.
Kelly, N. J., W. V. Boynton, K. Kerry, D. Hamara, D. Janes, I. Mikheeva, T. Prettyman, W. C. Feldman, and the GRS Team (2003), Preliminary thickness measurements of the seasonal polar carbon dioxide frost on Mars, paper presented at Sixth International Conference on Mars, Jet Propul. Lab., Pasadena, Calif.
Kieffer, H. H. (1979), Mars south polar spring and summer temperatures: A residual CO_2 frost, *J. Geophys. Res.*, *84*, 8263–8288.
Kieffer, H. H., and T. N. Titus (2001), TES mapping of Mars' north seasonal cap, *Icarus*, *154*, 162–180.
Kieffer, H. H., T. Z. Martin, S. C. Chase, E. D. Miner, and F. D. Palluconi (1976), Martian north pole summer temperatures—Dirty water ice, *Science*, *194*, 1341–1344.
Kieffer, H. H., T. N. Titus, K. F. Mullins, and P. R. Christensen (2000), Mars south polar spring and summer behavior observed by TES: Seasonal cap evolution controlled by frost grain size, *J. Geophys. Res.*, *105*, 9653–9699.
Leighton, R. R., and B. C. Murray (1966), Behavior of carbon dioxide and other volatiles on Mars, *Science*, *153*, 136–144.
Lemoine, F. G., D. E. Smith, D. D. Rowlands, M. T. Zuber, G. A. Neumann, D. S. Chinn, and D. E. Pavlis (2001), An improved solution of the gravity field of Mars (GMM-2B) from Mars Global Surveyor, *J. Geophys. Res.*, *106*, 23,359–23,376.
Leovy, C. B. (1985), The general circulation of Mars: Models and observations, *Adv. Geophys.*, *28a*, 327–346.
Martin, L. J., P. B. James, A. Dollfus, K. Iwasaki, and J. D. Beish (1992), Telescopic observations: Visual, photographic, polarimetric, in *Mars*, edited by H. H. Kieffer et al., pp. 34–70, Univ. of Ariz. Press, Tucson.
Mellon, M. T. (1996), Limits on the CO_2 content of the Martian polar deposits, *Icarus*, *124*, 268–279.
Mitrofanov, I. G., et al. (2003), CO_2 snow depth and subsurface water-ice abundance in the northern hemisphere of Mars, *Science*, *300*, 2081–2084.
Neumann, G. A., D. D. Rowlands, F. G. Lemoine, D. E. Smith, and M. T. Zuber (2001), Crossover analysis of Mars Orbiter Laser Altimeter data, *J. Geophys. Res.*, *106*, 23,753–23,768.
Neumann, G. A., J. B. Abshire, D. E. Smith, X. Sun, and M. T. Zuber (2002), MOLA 1064 nm radiometry measurements: Status and prospects in extended mission, *Proc. Lunar Planet. Sci. Conf. 33rd*, 1889.
Neumann, G. A., J. B. Abshire, O. Aharonson, J. B. Garvin, X. Sun, and M. T. Zuber (2003), Mars Orbiter Laser Altimeter pulse width measurements and footprint-scale roughness, *Geophys. Res. Lett.*, *30*(11), 1561, doi:10.1029/2003GL017048.
Nye, J. F., H. H. Wills, W. B. Durham, P. M. Schenk, and J. M. Moore (2000), The instability of a south polar cap on Mars composed of carbon dioxide, *Icarus*, *144*, 449–455.
Paige, D. A. (1992), The thermal stability of near-surface ground ice on Mars, *Nature*, *356*, 43–45.
Paige, D. A., and A. P. Ingersoll (1985), Annual heat balance of Martian polar caps—Viking observations, *Science*, *228*, 1160–1168.
Paige, D. A., and S. E. Wood (1992), Modeling the Martian seasonal CO_2 cycle. 2. Interannual variability, *Icarus*, *99*, 15–27.
Pollack, J. B., R. M. Haberle, and J. Schaeffer (1990), Simulations of the general circulation of the Martian atmosphere: 1. Polar processes, *J. Geophys. Res.*, *95*, 1447–1473.
Pollack, J. B., R. M. Haberle, J. Murphy, and H. Lee (1993), Simulations of the general circulation of the Martian atmosphere: 2. Seasonal pressure variations, *J. Geophys. Res.*, *98*, 3125–3148.
Press, W. H., S. A. Teukolsky, W. T. Vetterling, and B. P. Flannery (1992), *Numerical Recipes in C: The Art of Scientific Computing*, 2nd ed., Cambridge Univ. Press, New York.
Rafkin, S. C. R., R. M. Haberle, and T. I. Michaels (2001), The Mars Regional Atmospheric Modeling System: Model description and selected simulations, *Icarus*, *151*, 228–256.
Richardson, M. I., and R. J. Wilson (2002), A topographically forced asymmetry in the Martian circulation and climate, *Nature*, *416*, 298–301.
Rowlands, D. D., D. E. Pavlis, F. G. Lemoine, G. A. Neumann, and S. B. Lutchke (1999), The use of crossover constraint equations derived from laser altimetry in the orbit determination of Mars Global Surveyor, *Geophys. Res. Lett.*, *26*, 1191–1194.
Schofield, J. T., J. R. Barnes, D. Crisp, R. M. Haberle, S. Larsen, J. A. Magalhaes, J. R. Murphy, A. Seiff, and G. Wilson (1997), The Mars Pathfinder Atmospheric Structure Investigation/Meteorology, *Science*, *278*, 1752–1757.
Smith, D. E., M. T. Zuber, R. M. Haberle, D. D. Rowlands, and J. R. Murphy (1999), The Mars seasonal CO_2 cycle and the time variation of the gravity field: A general circulation model simulation, *J. Geophys. Res.*, *104*, 1885–1896.
Smith, D. E., M. T. Zuber, and G. A. Neumann (2001a), Seasonal variation of snow depth on Mars, *Science*, *294*, 2141–2146.
Smith, D. E., et al. (2001b), Mars Orbiter Laser Altimeter: Experiment summary after the first year of global mapping of Mars, *J. Geophys. Res.*, *106*, 23,689–23,722.
Tanaka, K. L., and D. H. Scott (1987), Geologic map of the polar regions of Mars, *U.S. Geol. Surv. Misc. Invest., Map I-1802C*.
Thomas, P., S. Squyres, K. Herkenhoff, A. Howard, and B. Murray (1992), Polar deposits of Mars, in *Mars*, edited by H. H. Kieffer et al., pp. 767–795, Univ. of Ariz. Press, Tucson.
Titus, T. N., H. H. Kieffer, K. F. Mullins, and P. R. Christensen (2001), TES premapping data: Slab ice and snow flurries in the Martian north polar night, *J. Geophys. Res.*, *106*, 23,181–23,196.
Titus, T. N., H. H. Kieffer, and P. R. Christensen (2003), Exposed water ice discovered near the south pole of Mars, *Science*, *299*, 1048–1051.
Toigo, A. D., and M. I. Richardson (2002), A mesoscale model for the Martian atmosphere, *J. Geophys. Res.*, *107*(E7), 5049, doi:10.1029/2000JE001489.
Wood, S. E., and D. A. Paige (1992), Modeling the Martian seasonal CO_2 cycle. 1. Fitting the Viking lander pressure curves, *Icarus*, *99*, 1–14.
Yoder, C. F., A. S. Konopliv, D. N. Yuan, E. M. Standish, and W. M. Folkner (2003), Fluid core size of Mars from detection of the solar tide, *Science*, *300*, 299–303.
Zuber, M. T., D. E. Smith, S. C. Solomon, D. O. Muhleman, J. W. Head, J. B. Garvin, J. B. Abshire, and J. L. Bufton (1992), The Mars Observer Laser Altimeter investigation, *J. Geophys. Res.*, *97*, 7781–7797.
Zurek, R. W., J. R. Barnes, R. M. Haberle, J. B. Pollack, J. E. Tillman, and C. B. Leovy (1992), Dynamics of the atmosphere of Mars, in *Mars*, edited by H. H. Kieffer et al., pp. 835–933, Univ. of Ariz. Press, Tucson.

O. Aharonson, California Institute of Technology, MC 150-21, Pasadena, CA 91125, USA. (oa@caltech.edu)

W. C. Feldman and T. H. Prettyman, Los Alamos National Laboratory, Mail Stop D466, Los Alamos, NM 87545, USA. (wfeldman@lanl.gov; thj@lanl.gov)

G. A. Neumann and D. E. Smith, Laboratory for Terrestrial Physics, NASA Goddard Space Flight Center, Code 920, Greenbelt, MD 20771, USA. (neumann@tharsis.gsfc.nasa.gov; dsmith@tharsis.gsfc.nasa.gov)

M. T. Zuber, Department of Earth, Atmospheric, and Planetary Sciences, Massachusetts Institute of Technology, 54-518, Cambridge, MA 02139, USA. (zuber@mit.edu)